

# Stray light suppression in spectroscopy using periodic shadowing

Elias Kristensson,<sup>1,\*</sup> Joakim Bood,<sup>1</sup> Marcus Alden,<sup>1</sup> Emil Nordström,<sup>1</sup> Jiajian Zhu,<sup>1</sup> Sven Huldt,<sup>2</sup> Per-Erik Bengtsson,<sup>1</sup> Hampus Nilsson,<sup>2</sup> Edouard Berrocal<sup>1</sup> and Andreas Ehn<sup>1</sup>

<sup>1</sup>Department of Physics, Lund University, Professorsgatan 1, SE-22363, Lund, Sweden

<sup>2</sup>Department of Astronomy and Theoretical Physics, Lund University, Sölvegatan 27, SE-22362, Lund, Sweden

[elias.kristensson@forbrf.lth.se](mailto:elias.kristensson@forbrf.lth.se)

**Abstract:** It is well known that spectroscopic measurements suffer from an interference known as stray light, causing spectral distortion that reduces measurement accuracy. In severe situations, stray light may even obscure the existence of spectral lines. Here a novel general method is presented, named Periodic Shadowing, that enables effective stray light elimination in spectroscopy and experimental results are provided to demonstrate its capabilities and versatility. Besides its efficiency, implementing it in a spectroscopic arrangement comes at virtually no added experimental complexity.

©2014 Optical Society of America

**OCIS codes:** (120.6200) Spectrometers and spectroscopic instrumentation; (170.5660) Raman spectroscopy; (300.1030) Absorption; (300.2140) Emission; (290.2648) Stray light.

## References and links

1. X. Qian, X.-H. Peng, D. O. Ansari, Q. Yin-Goen, G. Z. Chen, D. M. Shin, L. Yang, A. N. Young, M. D. Wang, and S. Nie, "In vivo tumor targeting and spectroscopic detection with surface-enhanced Raman nanoparticle tags," *Nat. Biotechnol.* **26**(1), 83–90 (2008).
2. H. Karttunen, P. Kröger, H. Oja, M. Poutanen, and K. J. Donner, *Fundamental Astronomy*, 5th ed. (Springer, 2007).
3. G. A. Kriss, J. M. Shull, W. Oegerle, W. Zheng, A. F. Davidsen, A. Songaila, J. Tumlinson, L. L. Cowie, J.-M. Deharveng, S. D. Friedman, M. L. Giroux, R. F. Green, J. B. Hutchings, E. B. Jenkins, J. W. Kruk, H. W. Moos, D. C. Morton, K. R. Sembach, and T. M. Tripp, "Resolving the Structure of Ionized Helium in the Intergalactic Medium with the Far Ultraviolet Spectroscopic Explorer," *Science* **293**(5532), 1112–1116 (2001).
4. D. Charbonneau, T. M. Brown, R. W. Noyes, and R. L. Gilliland, "Detection of an extrasolar planet atmosphere," *Astrophys. J.* **568**(1), 377–384 (2002).
5. D. Sudarsky, A. Burrows, and P. Pinto, "Albedo and reflection spectra of extrasolar giant planets," *Astrophys. J.* **538**(2), 885–903 (2000).
6. A. C. Eckbreth, *Laser Diagnostics for Combustion Temperature and Species*, 3rd ed. (Taylor and Francis, 1996).
7. C. N. Banwell, *Fundamentals of Molecular Spectroscopy*, 4th ed. (McGraw-Hill, 1994).
8. D. A. Long, *The Raman Effect: A Unified Treatment of the Theory of Raman Scattering by Molecules* (John Wiley, 2002).
9. A. C. Ferrari, J. C. Meyer, V. Scardaci, C. Casiraghi, M. Lazzeri, F. Mauri, S. Piscanec, D. Jiang, K. S. Novoselov, S. Roth, and A. K. Geim, "Raman Spectrum of Graphene and Graphene Layers," *Phys. Rev. Lett.* **97**(18), 187401 (2006).
10. J. M. Hollas, *Modern Spectroscopy*, 4th ed. (John Wiley, 2004).
11. V. A. Fassel, J. M. Katzenberger, and R. K. Winge, "Effectiveness of interference filters for reduction of stray light effects in atomic emission spectrometry," *Appl. Spectrosc.* **33**(1), 1–5 (1979).
12. P. W. J. M. Boumans, "A century of spectral interferences in atomic emission spectroscopy - Can we master them with modern apparatus and approaches?" *J. Anal. Chem.* **324**(5), 397–425 (1986).
13. G. F. Larson and V. A. Fassel, "Line broadening and radiative recombination background interferences in inductively coupled plasma-atomic emission spectroscopy," *Appl. Spectrosc.* **33**(6), 592–599 (1979).
14. R. Donaldson, "Stray light in monochromators," *J. Sci. Instrum.* **29**(5), 150–153 (1952).
15. S. Bykov, I. Lednev, A. Ianoul, A. Mikhonin, C. Munro, and S. A. Asher, "Steady-state and transient ultraviolet resonance Raman spectrometer for the 193–270 nm spectral region," *Appl. Spectrosc.* **59**(12), 1541–1552 (2005).
16. V. A. Fassel, "Quantitative elemental analyses by plasma emission spectroscopy," *Science* **202**(4364), 183–191 (1978).
17. S. Nie and S. R. Emory, "Probing single molecules and single nanoparticles by surface-enhanced Raman scattering," *Science* **275**(5303), 1102–1106 (1997).

18. P. W. J. M. Boumans, "Inductively coupled plasma-atomic emission spectroscopy: Its present and future position in analytical chemistry," *Fresenius J. Anal. Chem.* **299**(5), 337–361 (1979).
19. G. Larson, V. Fassel, R. Winge, and R. Kniseley, "Ultratrace analyses by optical emission spectroscopy: The stray light problem," *Appl. Spectrosc.* **30**(4), 384–391 (1976).
20. R. E. Poulsen, "Test methods in spectrophotometry: Stray-light determination," *Appl. Opt.* **3**(1), 99–104 (1964).
21. D. Landon and S. P. S. Porto, "A tandem spectrometer to detect laser-excited Raman radiation," *Appl. Opt.* **4**(6), 762–763 (1965).
22. G. Mestl, "In situ Raman spectroscopy – a valuable tool to understand operating catalysts," *J. Mol. Catal. Chem.* **158**(1), 45–65 (2000).
23. F. Tuinstra and J. L. Koenig, "Raman spectrum of graphite," *J. Chem. Phys.* **53**(3), 1126–1130 (1970).
24. D. G. Cameron and D. J. Moffatt, "A generalized approach to derivative spectroscopy," *Appl. Spectrosc.* **41**(4), 539–544 (1987).
25. M. L. Meade, "Advances in lock-in amplifiers," *J. Phys. E Sci. Instrum.* **15**(4), 395–403 (1982).
26. M. A. A. Neil, R. Juskaitis, and T. Wilson, "Method of obtaining optical sectioning by using structured light in a conventional microscope," *Opt. Lett.* **22**(24), 1905–1907 (1997).
27. H. Wu, J. V. Volponi, A. E. Oliver, A. N. Parikh, B. A. Simmons, and S. Singh, "In vivo lipidomics using single-cell Raman spectroscopy," *Proc. Natl. Acad. Sci. U.S.A.* **108**(9), 3809–3814 (2011).
28. S. Roy, J. R. Gord, and A. K. Patnik, "Recent advances in coherent anti-Stokes Raman scattering spectroscopy: Fundamental developments and applications in reacting flows," *Pror. Energy Combust. Sci.* **36**(2), 280–306 (2010).
29. M. Müller and A. Zumbusch, "Coherent anti-Stokes Raman scattering microscopy," *ChemPhysChem* **8**(15), 2156–2170 (2007).
30. B. von Vacano, L. Meyer, and M. Motzkus, "Rapid polymer blend imaging with quantitative broadband multiplex CARS microscopy," *J. Raman Spectrosc.* **38**(7), 916–926 (2007).
31. A. Bohlin, B. D. Patterson, and C. J. Kliewer, "Communication: Simplified two-beam rotational CARS signal generation demonstrated in 1D," *J. Chem. Phys.* **138**(8), 081102 (2013).

## 1. Introduction

Most fields within natural science benefit from optical spectroscopy, with wide applications such as detection of tumors [1], classification of stars and space exploration [2–5], species determination [6,7], identification of molecular and electronic structure [8,9], validation of physical models [10], etc. However, a common measurement obstacle in spectroscopy is the interference known as *stray light*, which, although lacking a strict definition, can be described as a general term comprising all spurious light reaching the detector in unintended ways, manifesting itself as background enhancements that vary across the wavelength range of the spectrum [11–21]. Optical components of the spectrograph, strong radiation and line wing overlap are often reported as the origins of stray light, but other effects may also factor in [11–15]. The implications of stray light distortion are many, including a worsened detection limit, analytical biases, concealment of weak spectral features, resolution losses, calibration errors, etc [11,12,15–17]. Despite the scientific endeavors during the last decades to overcome these issues, no conclusive and general solution to the problem has been found. Yet the ability to perform precise corrections for stray light is paramount for the prospect of new discoveries by means of spectroscopy.

Stray light distortions can be mitigated through the use of double or triple monochromators [13–15,21–23]. However, these are based on a scanning procedure and are therefore not only a costly and time-consuming solution, they also leave out the possibility of acquiring instantaneous two-dimensional (2D) spectra (i.e. spectrally- and spatially resolved information recorded simultaneously). In addition, all scanning instruments share one common complication: the need to monitor and compensate for variations in the brightness of the object. High-performance holographic notch filters are often employed to inhibit the detection of stray light, yet such filters account only for stray light caused by a specific source, emitting at a specific wavelength [22]. The selectivity of both these experimental approaches limits their number of applications considerably.

The most well known computer-aided approach for stray light correction is the derivative method, which attempts to solve the problem by extracting and analyzing derivatives of the spectrum [22,24]. The main benefit of this process is that broad spectral structures are suppressed relative sharper bands, thus permitting the identification of relatively weak features. However, derivatives are extremely sensitive to noise and rely heavily on smoothing, which is undesired since it deteriorates spectral resolution. Also, obtaining

optimum results for a given line-width require fine-tuning, which renders complications and uncertainties when the spectrum contains lines with variations in bandwidths.

In this article, we present a general method – Periodic Shadowing (PS) – for stray light elimination that is suitable for all spectrographs with stigmatic imaging properties, thus including nearly all modern instruments optimized for use of 2D detectors (or 1D sensor arrays).

## 2. Periodic shadowing

Periodic Shadowing, which is mainly inspired by lock-in amplification [25] (frequency modulation and phase-sensitive detection in the temporal domain) and Structured Illumination Microscopy [26] (employed in microscopic imaging to increase depth-resolution), strongly reduce the stray light problem by tagging the photons incident on the spectrograph with a certain, predefined pattern. The configuration being presented here utilizes a Ronchi (square wave) grid target, mounted at the entrance slit (Fig. 1(a)), to tag the light – no other modification to the hardware of the spectroscopic system is required.

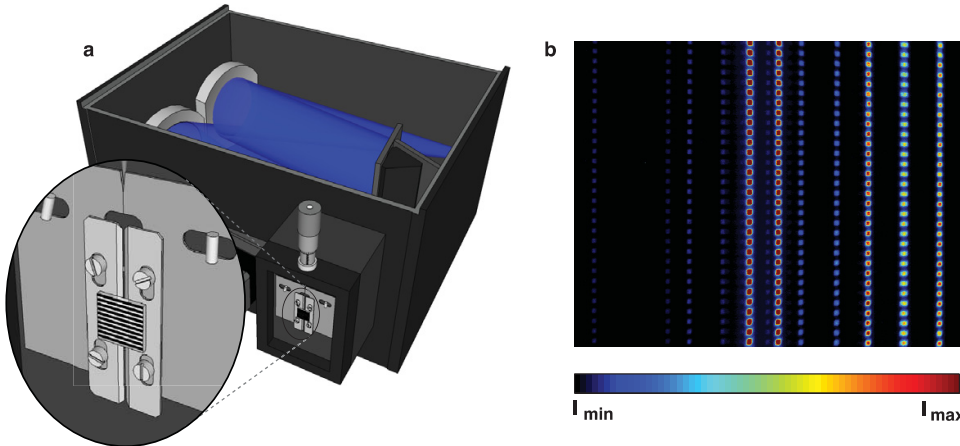


Fig. 1. Schematic view of the experimental arrangement. (a) The inserted Ronchi pattern at the entrance slit is the only hardware modification to the spectrograph. (b) Unprocessed PS spectrum of an argon discharge lamp in which the superimposed periodic shadows can be observed.

Owing to the fact that the entrance slit is imaged onto the detector at all wavelengths, the fine stripes of the Ronchi grid will effectively cast periodic shadows with a given spatial frequency and phase (along the slit direction), superimposed on all spectral lines (Fig. 1(b)). The stray light is, by definition, incapable of maintaining this well-defined structure during its passage through the spectrograph and will, in contrast to the signal photons, appear as a wavelength-dependent intensity offset on the detector. This distinction allows the signal photons to be identified and separated from the stray light, both in one and two-dimensional measurements, using a simple post-processing routine. We incorporate a lock-in detection algorithm [26] on each column of the acquired spectrum to extract only the information that appears with exactly the same periodicity as that of the Ronchi grid (procedure outlined in Appendix A). Apart from suppressing stray light, this approach also has the added benefit of reducing the impact of white noise. Furthermore, with the tagging process and data acquisition occurring simultaneously, pre-calibrations and blank- or background recordings are avoided.

## 3. Results and discussion

To experimentally verify the capabilities and versatility of the PS technique, four spectroscopic methods were studied, selected to achieve a high experimental diversity; (1) emission – where intense lines are known to give rise to locally elevated levels of stray light;

(2) absorption – where the added intensity from stray light lead to an underestimated absorption; (3) laser-induced scattering – where stray light from the intense laser line conceals spectral features; and (4) Coherent anti-Stokes Raman Spectroscopy – to demonstrate that PS can be applied in spectral analysis of coherent signals. Each set of experiment was compared with the corresponding conventional method.

### 3.1 Emission

To study natural emission the radiation from a cadmium discharge lamp was recorded, see Fig. 2. The benefits of this sample are that its emission is not particularly intense and the visible spectrum contains well-separated lines. Stray light contamination is thus expected to be moderate. Despite this, a large improvement in line contrasts is observed when comparing the PS and conventional spectrum (Fig. 2(a)). Figure 2(b) shows how the stray light contribution varies significantly across the spectrum, increasing by a factor of up to 300 in line-rich regions. As explained by Larson *et. al* [11], this local increase of stray light is due to a superposition of wings from strong emission lines and is particularly problematic to compensate for as the magnitude of the effect depends on the current – often unknown – state of the sample. However, if left unaccounted for these enhancements directly transfer into analytical errors, as is exemplified by the signal-to-background values (Figs. 2(c)–2(e)).

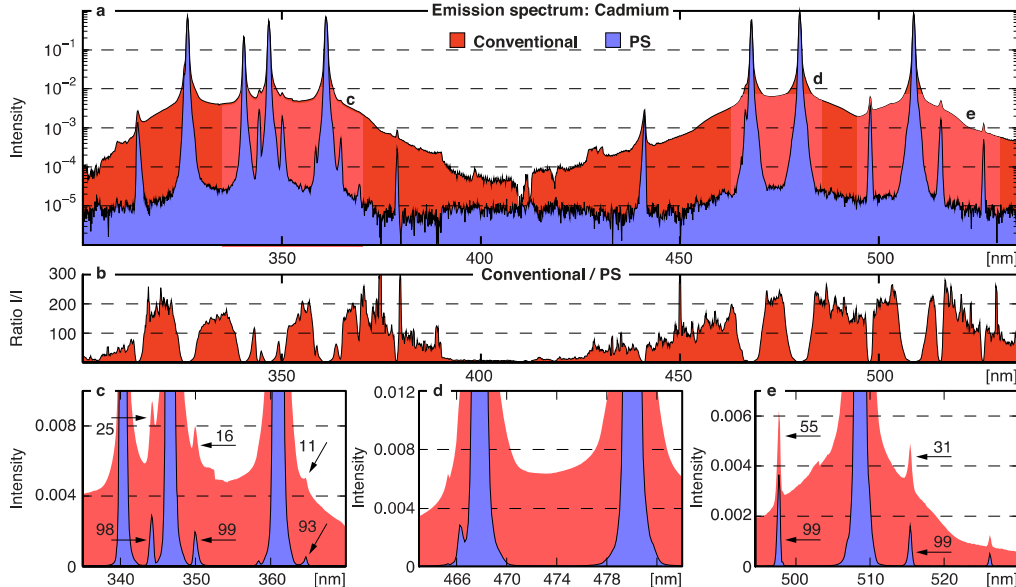


Fig. 2. Spectrum from a cadmium discharge lamp, acquired using both PS and conventional spectroscopy. (a) With its ability to distinguish between stray light and signal photons on a pixel level, PS generates a spectrum with line contrasts that greatly exceed the conventional ones (note the logarithmic scale). Both spectra are scaled between zero and unity. (b) Ratio between conventional and PS spectrum, revealing the complex structure of the stray light intensity, increasing nearby line-rich regions. This behavior demonstrates how the stray light level cannot be assessed indirectly by evaluating the baseline in vacant regions of the spectrum. (c)-(e) Weak spectral lines residing on the wings of strong emission lines are problematic to monitor accurately due to the locally elevated levels of stray light. PS significantly improves the signal-to-background values for such weak lines (indicated by the arrows).

### 3.2 Absorption

Astronomical observations rely almost entirely on passive methods, absorption and emission spectroscopy being among the most important ones [2] but where the former is particularly sensitive to stray light contamination. In a spectroscopic stellar measurement stray light

lowers the continuum level (broadband blackbody radiation) while filling the absorption lines, thus smoothening spectral features, in turn generating systematic errors in spectral-line widths, depths and shapes. A double or triple monochromator arrangement yields lower stray light levels, but these systems are generally avoided in astronomy nowadays (for the previously mentioned reasons) in favor of CCD-based systems. The ability to suppress stray light on a 2D arrangement thus makes PS promising for the prospect of increased sensitivity, which is key when weak spectral signatures are sought, e.g. when attempting to study the atmosphere of extrasolar planets [4,5]. Here a faint absorption imprint – only a fraction of the continuum level – is superposed on an overwhelmingly bright stellar spectrum and even minute spectral distortions due to stray light contamination are thus crucial to avoid. Figure 3 shows a high-resolution absorption spectrum of the sun where the benefits of the PS technique for absorption applications in general are demonstrated (note that, apart from subtracting the average intensity on either side of the stellar exposure in the conventional case, no other corrections were carried out in this measurement).

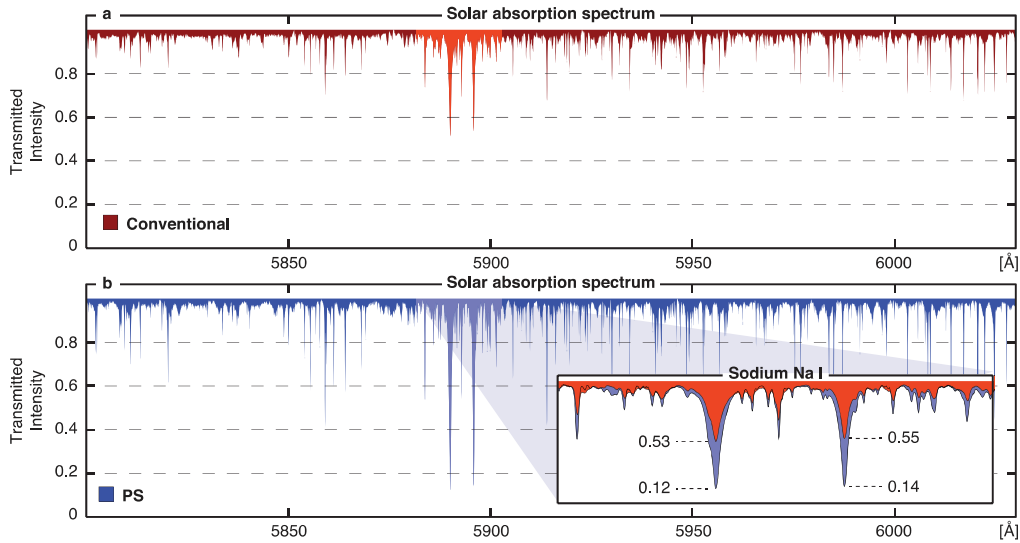


Fig. 3. Solar absorption spectrum, acquired using either conventional spectroscopy or PS. (a) Conventional spectrum of the sun. The significant amount of stray light is believed to arise from ruling deficiencies. (b) The corresponding PS spectrum, characterized by sharper, stronger absorption lines. The inset highlights the considerable difference in intensity for the prominent Fraunhofer lines of sodium at 5890 Å (D<sub>2</sub>) and 5896 Å (D<sub>1</sub>).

### 3.3 Scattering

One of the most frequently employed laser-induced methods within spectroscopy is Raman scattering – an inelastic process where the generated frequency shift permits species-specific measurements [8]. However, laser-induced Raman scattering measurements are often largely affected by stray light arising from the intense elastic scattering (Rayleigh, Mie and Tyndall scattering, as well as reflections) – often manifested as a broad, expanding wing. Because of this and the relatively low scattering Raman cross-section, stray light interference has been a long-standing complication for Raman spectroscopy and transitions at low wavenumbers are rarely included in the analysis [15,17,22,23,27]. Figure 4 illustrates how the transitions near the laser wavelength become readily accessible by means of PS, thus opening up for new measurement routines and identification procedures. Experimental and theoretical spectra show excellent agreement (Figs. 4(c) and 4(d)), confirming a proper operation of the PS method. However, since PS is primarily a post-processing tool, sharp notch filters may still be required in laser-based applications to diminish the strong laser radiation and to improve the signal-to-noise ratio (S/N).

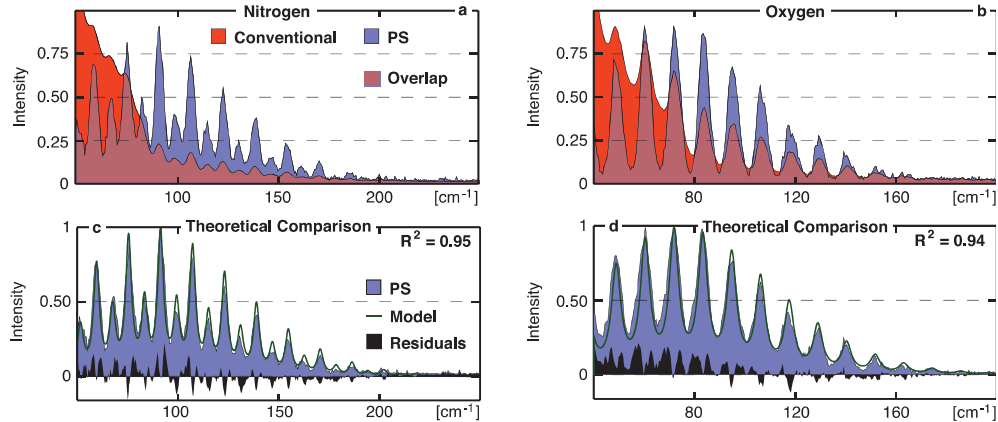


Fig. 4. Comparison between PS and conventional laser-induced rotational Raman spectroscopy in a gaseous medium. (a) and (b) Raman spectra of pure nitrogen and oxygen, respectively. Since Raman scattering is considerably weaker than Rayleigh scattering, stray light suppression becomes a necessity for the detection of Raman transitions at low wavenumbers. Mie and Tyndall scattering as well as reflections are also contributing to the elastic light in most practical measurement situations. The PS data illustrates the prospect of increasing the operating range of Raman spectroscopy, to permit accurate monitoring of lines closer to the laser line. (c) and (d) Theoretical Raman spectra fitted against PS spectra, showing excellent agreement.

### 3.4 Coherent signals

Similar to Raman scattering, coherent anti-stokes Raman spectroscopy (CARS) is also a laser-based technique that provides species-specificity, used for both micro- and macroscopic applications [6,28–30]. However, the signal generated in CARS is, in contrast to Raman scattering, coherent and has laser-like characteristics, thus permitting additional schemes for stray light suppression based on polarization, long optical paths and sharp, optical filters. Further, in situations when the acquired data still suffer from errors induced by stray light, the laser configuration of CARS (wave-mixing of laser beams with different wavelengths) allows the background offset to be measured in a separate recording. A PS spectrum, acquired at such measurement conditions using a two-beam rotational CARS configuration [31], is displayed in Fig. 5(a) accompanied by raw data as well as background-corrected CARS data. The residual signal, in Fig. 5(b), shows an excellent agreement between the two differently processed data sets, demonstrating both that background acquisitions in CARS – when required – can be circumvented by means of PS (Figs. 5(a) and 5(c)) and that PS is applicable for the analysis of coherent signals. Apart from being more time efficient, the greatest merit of PS for CARS experiments is arguably the possibility of recording single laser shot spectra, even in harsh environments where e.g. beam-steering and changes in polarization gives rise to temporal fluctuations in the stray light contribution (Fig. 5(d)).

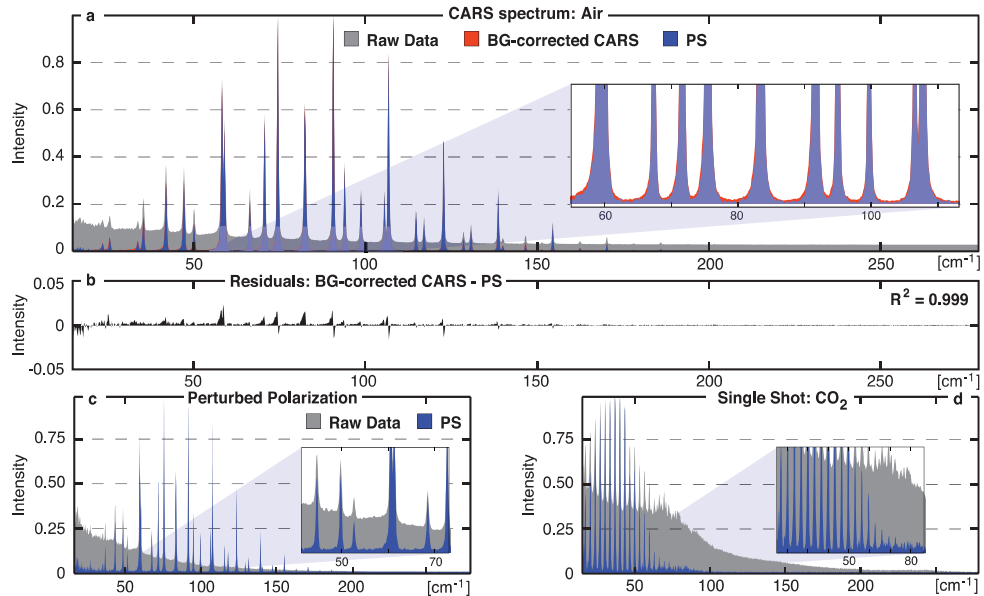


Fig. 5. Comparison of rotational CARS spectra acquired using either PS or conventional spectroscopy. (a) CARS evaluation is commonly made on a signal spectrum from which a background spectrum (recorded while blocking the Stokes beam) is subtracted. By implementing PS, the requisite for such a second measurement is circumvented. (b) Residual plot, showing the close agreement between background-corrected CARS and PS, experimentally verifying a proper operation of PS for coherent signals. (c) Example of a spectrum from a two-beam CARS measurement, where the polarization of the spatially overlapping probe beam is perturbed as it passes through an optical window, in an attempt to mimic undesired effects commonly encountered in e.g. high-pressure measurements, where optical ports are a necessity. (d) Example of an instantaneously acquired  $\text{CO}_2$  spectrum, recorded under similar conditions. Due to temporal fluctuations of the conditions in the measurement volume, accurate background readings cannot be attained without PS.

### 3.5 Signal to noise

Losing light is an inevitable side effect of all modulation schemes. In the case of PS the inserted Ronchi grid blocks about half of the incident light, thus potentially reducing the S/N by an equal amount. However, the *a priori* characteristics of the signal of interest – its unique spatial phase and frequency – can be exploited to reduce noise. Two processes are mainly responsible for the filtering of noise. First, the signal is shifted to a less noisy environment (high spatial frequency), thus reducing the influence of white noise. Second, a (spatial) band-pass filter is applied on the signal, removing redundant spatial frequencies that otherwise add noise. This noise-filtering capability is illustrated in Fig. 6, showing statistical analysis on a CARS measurement of air. Analysis of regions free from spectral lines revealed a reduction of the noise by at least a factor of two when implementing PS (Fig. 6), thus fully compensating, in terms of S/N, for the loss of light introduced by the Ronchi grid.

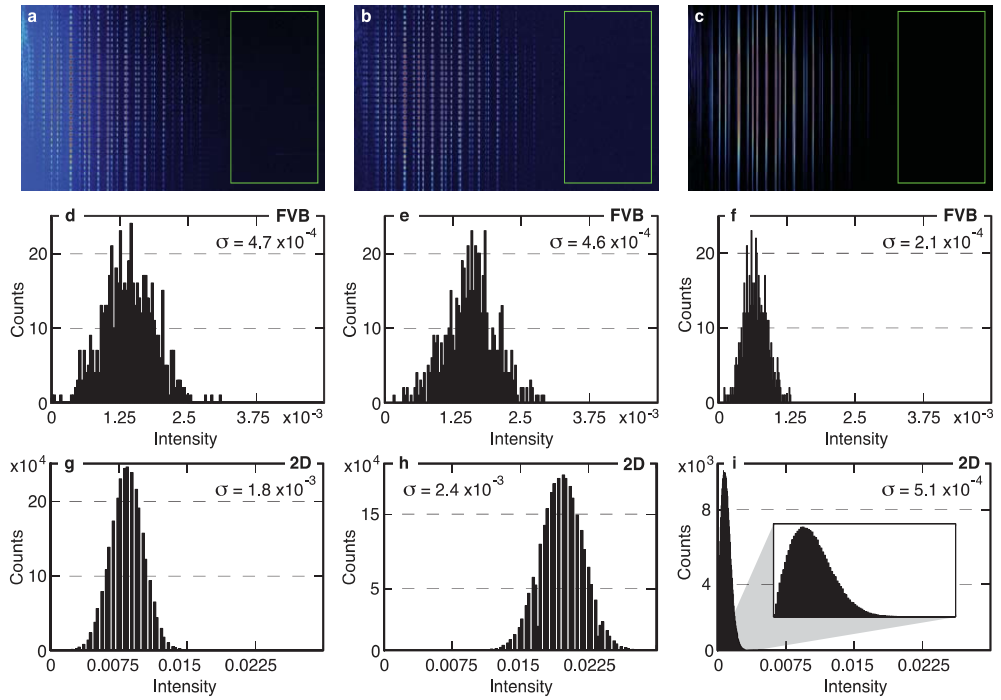


Fig. 6. Comparison of the noise levels for rotational CARS spectra of air. (a) Unprocessed CARS spectrum. (b) Background-corrected CARS spectrum. (c) Corresponding PS spectrum. The green frame indicates the region of interest (ROI) for the analysis, chosen for being free of spectral lines. Each spectrum is normalized prior to the statistical analysis, having values between zero and unity. The S/N can therefore be estimated directly from the noise level (being inversely proportional to the standard deviation). (d)-(f) Histograms of the ROI after full vertical binning (FVB), revealing a reduction of the noise by approximately a factor of 2 with PS. (g)-(i) Histograms of the ROI with no pixel binning, suggesting an even greater improvement in S/N.

#### 4. Conclusion

In conclusion, a novel spectroscopic method, having the capability of suppressing stray light, has been described and experimentally demonstrated. The basic principle of the method consists of applying a pattern that blocks light with a certain periodicity against the entrance slit of the spectrometer. This predefined transmission characteristic is only maintained by photons traveling the correct optical path through the spectrometer, thus making stray light and signal photons distinguishable in the acquired spectrum. To extract the signal photons and suppress the unwanted stray light, we incorporate a spatial lock-in algorithm, which also has noise-filtering benefits.

Besides its ability to suppress stray light, Periodic Shadowing is inexpensive and adds nearly no experimental complexity to the spectroscopic setup.

## Appendix A: Lock-in Analysis

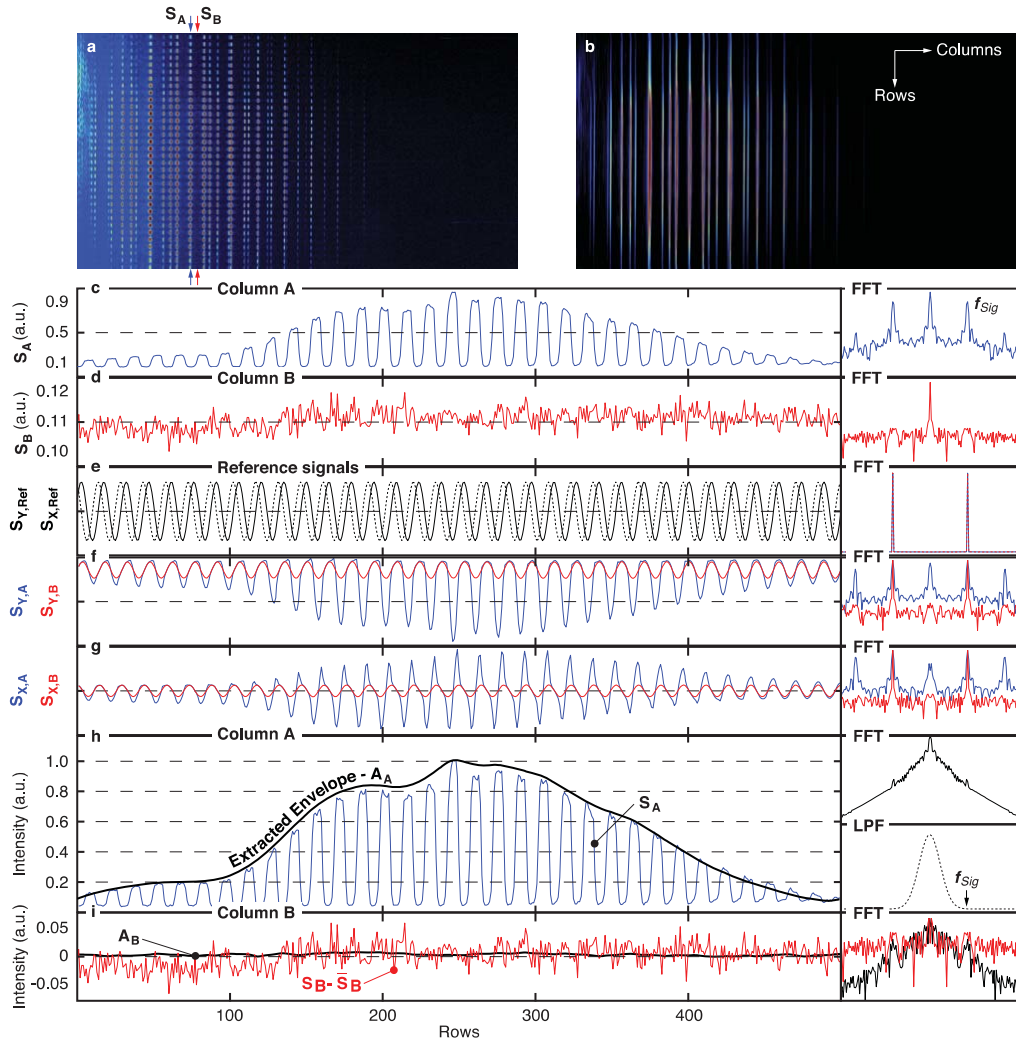


Fig. 7. Example of the processing steps of PS. Each graph is accompanied by its corresponding Fourier transforms, all shown in a logarithmic scale (x-axis truncated). (a) Unprocessed rotational CARS spectrum. (b) Corresponding PS spectrum. (c) Intensity variations along the columns “A” (blue). (d) Intensity variations along the columns “B” (red). (e) References signals, 90 degrees shifted in phase. (f) Product of the first reference signal and both “A” and “B”. (g) Product of second reference signal and both “A” and “B”. (h) Result of the PS algorithm, which extracts the envelope ( $A_A$ ) of column “A”. The low-pass filter (LPF) is shown in a linear scale. (i) Difference in noise level (column B) between PS (black) and conventional spectroscopy (red), where the latter is offset-adjusted, for reasons of clarity.

The lock-in analysis outlined in this appendix is graphically represented in Fig. 7. To be able to use lock-in detection algorithms in the data post-processing of PS the signal must be modulated with a well-defined spatial frequency. In PS, this frequency,  $f_{Sig}$ , is set by the magnification (or demagnification) of the Ronchi ruling, which typically has 5-20 periods/mm. Although remaining constant, we routinely determine  $f_{Sig}$  from each data set through Fourier analysis, where the software simply assumes  $f_{Sig}$  to be the strongest non-zero component in the Fourier domain (for optimum performance it is advised to exclude low spatial frequencies in the analysis to avoid ambiguities caused by the  $1/f$  noise). With  $f_{Sig}$

being determined, each column,  $S_C$ , of the 2D spectrum (Fig. 7(a)) is then analyzed separately. This signal vector can be expressed as

$$S_C(R) = A_C(R) \sin(2\pi f_{Sig} R + \varphi_C) + B_C(R) \quad (1)$$

The row index,  $R$ , and column index,  $C$ , are integer numbers. In this formulation the signal is divided into two parts; (1) the frequency modulated part,  $A_C(R)$ , which basically contains the signal of interest (SOI), and (2) a non-modulated offset,  $B_C(R)$ , arising from various sources of noise and interference. If we assume that  $f_{Sig}$  remains constant for all columns – a reasonable assumption in PS – two reference signals,  $S_{X,Ref}$  and  $S_{Y,Ref}$  (see Fig. 7(e)) can be formed as

$$S_{X,Ref}(R) = \sin(2\pi f_{Sig} R + \varphi_{Ref}) \quad (2)$$

and

$$S_{Y,Ref}(R) = \sin(2\pi f_{Sig} R + \varphi_{Ref} + \pi/2) \quad (3)$$

where the phase shift of  $\pi/2$  is the only difference between the two. Multiplying the signal vector,  $S_C$ , with the two reference signals leads the following signal vectors (see Figs. 7(f) and 7(g)).

$$S_{X,C}(R) = S_C(R) \cdot S_{X,Ref} = \frac{1}{2} A_C(R) [\cos(\varphi_C - \varphi_{Ref}) - \cos(4\pi f_{Sig} R + \varphi_C + \varphi_{Ref})] + B_C(R) \sin(2\pi f_{Sig} R + \varphi_{Ref}) \quad (4)$$

$$S_{Y,C}(R) = S_C(R) \cdot S_{Y,Ref} = \frac{1}{2} A_C(R) [\sin(\varphi_C - \varphi_{Ref}) - \sin(4\pi f_{Sig} R + \varphi_C + \varphi_{Ref})] + B_C(R) \sin(2\pi f_{Sig} R + \varphi_{Ref} + \pi/2) \quad (5)$$

Applying a low-pass filter with a cut-off frequency of  $f_C = f_{Sig}$  (lower right panel in Fig. 7(h)) on these vectors (ideally) removes the modulated components, resulting in two new vectors,

$$X_C(R) = \frac{1}{2} \tilde{A}_C(R) \cos(\varphi_C - \varphi_{Ref}) \quad (6)$$

and

$$Y_C(R) = \frac{1}{2} \tilde{A}_C(R) \sin(\varphi_C - \varphi_{Ref}) \quad (7)$$

where the tilde assignment on  $A_C$  is due to the frequency filtering. In the presented results, we apply a pure Gaussian to reject higher spatial frequencies. The SOI is finally determined by calculating

$$\tilde{A}_C(R) = 2\sqrt{X_C(R)^2 + Y_C(R)^2} \quad (8)$$

which basically extracts the envelope of  $S_C$  (Fig. 7(h)).

Analyzing the data using lock-in algorithms leads to a slight loss of spatial resolution, the magnitude of which is inversely proportional to the spatial frequency of the Ronchi grating. Selecting a Ronchi grating with high spatial frequency is therefore advised to minimize the loss of spatial resolution. However, 2D PS spectroscopy with no loss of spatial resolution can be achieved by shifting the Ronchi grating physically in space, following the methodology described by Neil *et al.* [26]. By shifting the grating and thereby the spatial phase of the shadow structure, the information previously hidden in the shadows becomes accessible.

Recording three spectra with relative spatial phases  $0$ ,  $2\pi/3$  and  $4\pi/3$  is sufficient for a full demodulation, according to

$$PS = \sqrt{(I_0 - I_{2\pi/3})^2 + (I_0 - I_{4\pi/3})^2 + (I_{2\pi/3} - I_{4\pi/3})^2} \quad (9)$$

where  $I_X$  is a 2D spectrum and the subscript  $X$  denote the spatial phase (in radians) of the shadows.

### Acknowledgments

This work was supported by the Linné Center within the Lund Laser Center (LLC) as well as the Center for Combustion Science and Technology (CECOST) through the Swedish Energy Agency. Also the European Research Council (ERC) Advanced Grant DALDECS is acknowledged. The authors gratefully acknowledge Dainis Dravins, Nils Ryde, Jerome Workman and Sune Svanberg for helpful discussions.